PHYSICAL REVIEW LETTERS

# Controlling Polarization Dynamics in a Liquid Environment: From Localized to Macroscopic Switching in Ferroelectrics

B. J. Rodriguez,[1] S. Jesse,[1] A. P. Baddorf,[1] S. -H. Kim,[2] and S. V. Kalinin[1,*]

[1]*Materials Science and Technology Division and The Center for Nanophase Materials Science, Oak Ridge National Laboratory, Oak Ridge, Tennessee 37831, USA*
[2]*Inostek Inc., Gyeonggi 426-901, Korea*

The effect of disorder on polarization switching in ferroelectric materials is studied using piezoresponse force microscopy in a liquid environment. The spatial extent of the electric field created by a biased tip is controlled by the choice of medium, resulting in a transition from localized switching dictated by tip radius, to uniform switching across the film. In the localized regime, the formation of fractal domains has been observed with dimensionality controlled by the length scale of the frozen disorder. In the nonlocal regime, preferential nucleation at defect sites and the presence of long-range correlations has been observed.

Electric-field induced polarization reversal is directly related to the elementary mechanisms of electron-lattice coupling and soft phonon mode behavior in ferroelectric materials [1] and is the functional basis for applications such as nonvolatile memories [2,3] and high-density data storage [4,5]. Polarization-dependent chemical etching and metal photodeposition reactions enable additional applications for nanofabrication [6,7]. These applied and fundamental considerations have generated broad interest towards understanding the elementary processes involved in polarization switching, such as domain nucleation, growth, and wall motion, and the role of defects, surfaces, and disorder on these processes [1–3].

In his seminal work, Landauer [8] demonstrated that the experimentally observed fields required for polarization switching correspond to unrealistically large values ($\sim 10^3$–$10^5$ kT) for the activation energy for domain nucleation. This observation, referred to as the Landauer paradox, necessitated the prediction of the presence of switching centers at which nucleation is initiated [1]. The spatial and energy distributions of the nucleation sites and the relative rates of nucleation versus domain growth processes are integral components of all modern theories describing macroscopic polarization switching. The interpretation of macroscopic switching data in the framework of Kolmogorov-Avrami-Ishibashi (KAI) [9] models often requires the use of fractional dimensionality to describe the geometry of the switching process [10,11]. However, despite almost 50 years of research, the spatial and energy distributions of the nucleation centers, the geometry of the growing domain, and the effect of disorder on domain geometry and dimensionality have remained enigmatic.

In the last decade, piezoresponse force microscopy (PFM), based on the direct probing of local electromechanical coupling in a piezoelectric material using a periodically biased atomic force microscope (AFM) tip [12,13], has emerged as a powerful tool for the nanoscale

characterization of ferroelectric materials. Application of a positive (negative) dc bias pulse to a conductive AFM tip in contact with a positively (negatively) polarized domain, results in a highly localized electric field, which induces the nucleation and subsequent growth of an oppositely polarized domain. Measurements of domain radii as a function of the amplitude and duration of voltage pulses provide information on the domain growth kinetics and bias dependence of the domain wall velocity. In ambient, the rapid $1/r$ decrease of the electric field with distance from the tip-surface junction results in the nucleation of a single domain located below the tip; i.e., the tip acts as the dominant nucleation center. At the same time, in ferroelectric capacitors, the presence of the top electrode limits the spatial resolution and affects the switching behavior, thus hindering the conclusive identification of defect sites.

Here, we explore PFM imaging and polarization dynamics in a liquid environment as a means to control the spatial extent of the electric field induced by the tip, and hence the mechanism of the switching process. Previously, we demonstrated PFM *imaging* in liquid with sub-10 nm resolution [14]. In this Letter, the effects of the conductive properties of the liquid on the switching behavior are explored. Solvent conductivity determines the spatial extent of the tip-induced potential distribution in the solution and hence the lateral spatial distribution of the normal component of the electric field in the film.

Liquid PFM was implemented on a commercial AFM system using a modified commercial liquid cell [14]. Switching studies in $(PZT)_{0.95}(BiFeO_3)_{0.05}$ (PZT-BFO) sol-gel thin films were performed in distilled water, $10^{-4}$, $10^{-3}$, $10^{-2}$, and $10^{-1}$ M NaCl solutions, and ethanol, methanol, isopropanol, and hexane. Surface topography of the film is shown in Fig. 1(a) and illustrates the presence of $\sim 30$ nm diameter grains. As in air, liquid PFM measurements are performed by applying a modulation voltage to a tip in contact with a piezoelectric surface. The electric
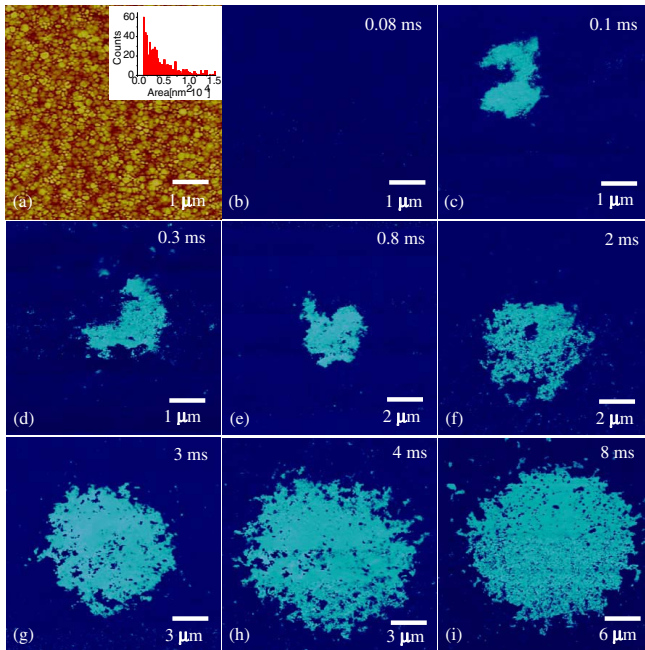
FIG. 1 (color online).   (a) Surface topography of the PZT-BFO film. The inset shows the characteristic grain size distribution. (b)–(i) Evolution of the switched domain in isopropanol as a function of pulse length for $-10$ V magnitude. The film is uniformly poled for 3 s by $+6$ V after each step. The phase contrast is 180°.

field generated at the tip-surface junction deforms the piezoelectric surface, which deflects the tip. The amplitude and phase of the tip oscillation are recorded simultaneously with topography. The PFM amplitude is proportional to the tip deflection (surface displacement) while the phase reveals the orientation of the polarization of the material. Polarization switching was performed by applying voltage pulses of a predefined amplitude and length to the tip in contact with the surface or raised above the surface.

The switching mode strongly depends on the solvent. In conductive solvents, switching requires the application of voltage pulses for several seconds and results in domain nucleation uniformly across the film area. The application of a sufficiently high bias results in complete polarization switching in the film. These switching regimes are referred to as partial and complete nonlocal switching, respectively. In air (and presumably in less conductive solvents, if a good tip-surface contact is established), the nucleation and growth of a single domain below the tip is possible. Remarkably, we note that imaging is possible in solvents such as $\sim 10^{-4}$ M NaCl in $H_2O$, distilled $H_2O$, $CH_3OH$, $C_2H_5OH$. Localized switching was achieved in isopropanol and methanol. However, in the latter, switching was associated with electrochemical reactions. We attribute this behavior to the difference in time scales involved in imaging ($\sim 1$ $\mu$s) and switching (1 ms–1 s) processes, sufficient for the onset of current flow and electrochemical reactions. In hexane, imaging was also possible, but no switching was

observed due to electrochemical reactions and sample degradation.

A particularly rich gamut of switching regimes was observed in isopropanol, which was thus chosen for detailed studies. The evolution of the domain size and geometry with pulse length is shown in Fig. 1(b)–1(i). Note that the domain boundaries are highly irregular, domain nucleation occurs outside the central area, and residual, unswitched domains remain within it. The sign of the switched domain is the same as under ambient conditions, where the application of a positive bias generates a domain with polarization pointing into the film.

To address the evolution of the domain geometry in the switching process, we have analyzed the fractal dimensionality of the switched domain using $P = \mu S^{D/2}$, where $P$ is the perimeter length, $\mu$ is a prefactor, $S$ the sampling area, and $D$ is dimensionality [15]. The log-log plot of the area versus perimeter length scale is shown in Fig. 2(a). The Rayleigh two point resolution [16] in the PFM image is estimated as $\sim 25$ nm and is comparable to the pixel size even for the smallest scans (20 nm), ensuring the veracity of the fractal dimensionality analysis. The minimum length scale for fitting was chosen to be above $\sim 3$ pixels in order to satisfy the Nyquist criterion.

The evolution of fractal dimensionality and effective size versus pulse parameters is shown in Fig. 2(b). Notice that for smaller ($<1$ $\mu$m) clusters, $D = 1.4$. The bulk value for the dimensionality is expected to be $D_{3D} = 2.5$.[10] Hence, the values obtained are in good agreement with those anticipated for the domain intersection with a sample surface, $D_{2D} = D_{3D} - 1$. The dimensionality in-
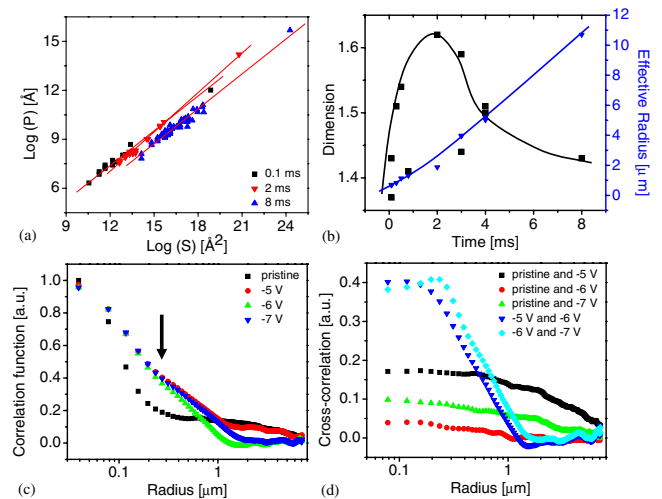


FIG. 2 (color online).   (a) Fractal plot of perimeter length after 0.1 ms (■), 2 ms (▼), and 8 ms (▲) pulses. The slope provides the fractal dimensionality of the switched domain. (b) Evolution of fractal dimension and characteristic domain size with the pulse length. The solid line is a guide to the eye. (c) Self-correlation functions after nonlocal switching. (d) Cross-correlation functions between different switched states.

creases to $D = 1.6$ for $\sim 2$ $\mu$m clusters and decreases again for larger clusters. We attribute this behavior to the interplay between the effective size of the switched area and frozen disorder in the film, where the dimensionality is maximum when the cluster size is comparable to the characteristic length scale of the disorder related to the polycrystalline nature of the film.

Variant switching scenarios arise for (a) more conductive solvents [e.g., ethanol, methanol], (b) tips with damaged coating, or (c) switching with the tip raised above the surface. In these cases, the dc field in solution, and hence the electric field across the film thickness, is essentially uniform, allowing the local defects to dominate the switching behavior. In ambient, the influence of defects on phase transitions, domain distributions, and domain wall kinetics has been studied by PFM [17–19]. In this case, the dc biased solution acts as a uniform liquid electrode, whereas the tip acts as a high resolution ($\sim 10$ nm) polarization sensor allowing direct imaging of the nucleation sites. An example of the evolution of the domain structure under nonlocal switching conditions in case (b) is shown in Fig. 3 [20]. Initially, the film is randomly polarized with domain sizes comparable to the grain size as shown in the PFM phase image, Fig. 3(a). The self-correlation function $C(r)$ of the PFM phase image is shown in Fig. 2(c). The application of a positive bias pulse results in uniform switching of the film [Fig. 3(b)]. Switching also requires longer times ($\sim 3$ s compared to $\sim 1$ ms for localized switching), as limited by the $RC$ time constant of the liquid cell (i.e., the tip-liquid-film-ground capacitor and the solution and sample resistances). The evolution of a switched pattern at increasing pulse magnitudes, and with fixed length ($t = 3$ s) is shown in Fig. 3(c)–3(f). The film was reset to a positive state [Fig. 3(b)] between each switching step. The self-correlation functions in Fig. 2(c) show that the char-
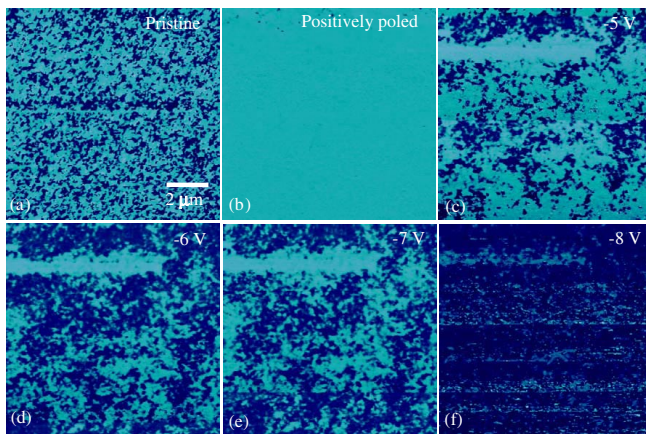
acteristic length scale of the switched domains ($\sim 300$ nm) is significantly larger than the grain size (30 nm), indicative of the presence of long-range correlations. The cross-correlation functions $C_{12}(r)$ between the initial (1) and the switched (2) states in Fig. 3(a) and 3(d) indicate that there is virtually no correlation. However, the cross-correlation functions between the images in Fig. 3(c) and 3(d) show clear correlation, despite the resetting of polarization state between images. This indicates that the disorder responsible for domain nucleation is frozen and related to the material microstructure rather than being stochastic in nature. This similarity is obvious upon visual comparison of Figs. 3(d) and 3(e). Qualitatively similar behavior was observed in ethanol and methanol; however, in these cases, detailed studies were hindered by concurrent electrochemical processes.

From these observations, the following picture of solvent-controlled tip-induced polarization switching emerges. In an ambient or nonconductive liquid environment, the biased tip establishes a highly localized electric field that decays rapidly with distance from the tip-surface junction. This field results in highly localized polarization switching above a certain threshold value, generating well-defined 2D domains that grow in area with pulse duration and magnitude, as shown schematically in Fig. 4(a). In this case, domain dimensionality is controlled by the field structure and is unaffected by large-scale disorder.

In a conducting liquid, the PFM contrast is strongly mediated by the presence of mobile ions that result in an increase of the effective area affected by the tip field [14]. For solvents with intermediate conductivities, the electric field is localized to the tip-surface junction, but the characteristic length scale is significantly larger than the tip size. The spreading resistance of the solution can be written as $R_{sol} = r_1/a$, where $r_1$ is the specific resistance of the solution and $a$ is the contact area, while the resistance of the film is $R_{film} = r_2 d/a^2$, where $r_2$ is the specific resistance of the film and $d$ is the film thickness. Assuming that switching occurs if the potential exceeds a critical value, $V_{crit}$, the size of the switched domain can be estimated as $a = (V_{tip} - V_{crit})r_2 d/(V_{crit}r_1)$. The switching in this case results in the formation of irregular fractal domains with scale-dependent dimensionality determined by the relationship between the domain size and the characteristic length scale of the frozen disorder, as shown in Fig. 4(b). In conductive solvents, the solution is uniformly biased, resulting in a homogeneous electric field across the film thickness (similar to ferroelectric capacitors), as shown schematically in Fig. 4(c). In this nonlocal case, the switching is dominated by the frozen disorder in the film, since the driving force for switching is independent of the position of the tip. Variation of the pulse length and magnitude in this case allows the regions where the switching is most likely to occur, i.e., the nucleation centers, to be visualized.



FIG. 3 (color online). Domain evolution during nonlocal switching in isopropanol. (a) Pristine film, (b) uniformly polarized film ($+6$ V for 5 s) and after (c) $-5$ V, (d) $-6$ V, (e) $-7$ V, and (f) $-8$ V pulses for 3 s. The film was switched to a uniform state after each step.
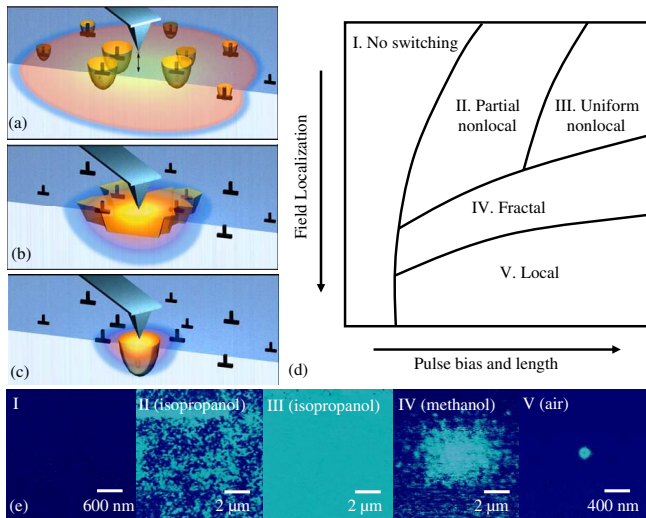
FIG. 4 (color online). Schematics of switching in (a) nonlocal, (b) fractal, and (c) local cases. The characteristic distribution of the electric field produced by the tip vs the nucleation site spacing and the resulting nucleation pattern are shown for each case. Field localization is controlled by the solvent conductivity and the tip-surface separation. (d) Schematic parameter diagram of possible switching modes vs field localization and pulse parameters. (e) PFM phase images illustrating domain morphology in regions I–V and the choice of solvent.

The evolution of the switching mechanism with solvent and bias parameters is illustrated in Fig. 4. Notably, high resolution *imaging* is possible even in conductive solvents because of the higher excitation frequencies that preclude the onset of electrochemical reactions and localization of the electromechanical interactions which transmit predominantly through the mechanical (rather than electrical) contact area. This allows *imaging* domains independently of whether the switching under similar conditions is local or nonlocal.

For the particular case of the PZT-BFO films studied in this work, we have observed that the characteristic length scale of the disorder, as deduced from the domain size of maximal dimensionality in the localized switching case and the correlation function analysis in the uniform switching case, is well above that of the grain size and is indicative of the presence of longer-range correlations, possibly mediated by elastic interactions through the substrate. In this respect, we note that similar behavior was observed in the spatial variability of switched current versus capacitor size [21].

To summarize, we have demonstrated the use of liquid PFM to control the mechanism of polarization switching. The screening of the applied field results in the localization of the high frequency ac field to the tip-surface junction and improved resolution during imaging [14]. The switching process is controlled by the low frequency field distribution. This allows the length and time scales for imaging and switching processes to be decoupled for subsequent

study. We believe that this capability to decouple imaging and switching processes through the control of the solvent opens a pathway to directly observe the spatial structure of the domains in the polarization switching process, thus allowing the dimensionality of the process and the disorder-mediated domain dynamics to be determined and ultimately the nucleation centers responsible for the Landauer paradox to be visualized. The use of liquid electrodes of controlled chemical reactivity allows opportunities to study localized ferroelectric fatigue behavior, the screening effects on the stability of ferroelectric nanodomains, and polarization mediated electro- and photochemical processes.

*Corresponding author.
sergei2@ornl.gov

[1] M. E. Lines and A. M. Glass, *Principles and Applications of Ferroelectric and Related Materials* (Clarendon, Oxford, 1977).
[2] J. Scott, *Ferroelectric Memories* (Springer-Verlag, Berlin, 2000).
[3] *Nanoelectronics and Information Technology*, edited by R. Waser (Wiley-VCH, Berlin, 2003).
[4] T. Tybell, C. H. Ahn, and J.-M. Triscone, Appl. Phys. Lett. **72**, 1454 (1998).
[5] Y. Cho *et al.*, Nanotechnology **17**, S137 (2006).
[6] K. Nassau, H. J. Levinstein, and G. M. Loiacono, Appl. Phys. Lett. **6**, 228 (1965).
[7] S. V. Kalinin *et al.*, Adv. Mater. **16**, 795 (2004).
[8] R. Landauer, J. Appl. Phys. **28**, 227 (1957).
[9] Y. Ishibashi and Y. Takagi, J. Phys. Soc. Jpn. **31**, 506 (1971).
[10] J. F. Scott, J. Phys. Condens. Matter **18**, R361 (2006).
[11] J. F. Scott, arXiv:cond-mat/0609023.
[12] P. Günther and K. Dransfeld, Appl. Phys. Lett. **61**, 1137 (1992).
[13] *Nanoscale Characterization of Ferroelectric Materials*, edited by M. Alexe and A. Gruverman (Springer, New York, 2004).
[14] B. J. Rodriguez *et al.*, Phys. Rev. Lett. **96**, 237602 (2006).
[15] WSxM©, http://www.nanotec.es.
[16] S. V. Kalinin *et al.*, Nanotechnology **17**, 3400 (2006).
[17] V. Likodimos *et al.*, Phys. Rev. B **63**, 064104 (2001).
[18] C. S. Ganpule *et al.*, Phys. Rev. B **65**, 014101 (2001).
[19] T. Tybell *et al.*, Phys. Rev. Lett. **89**, 097601 (2002).
[20] C. Ganpule, Ph.D. thesis, University of Maryland, 2001.
[21] S. Sommerfelt (private communications).